Chemical pressure and magnetic field effects in CePtGa

2007 J. Phys.: Condens. Matter 19 506211

(http://iopscience.iop.org/0953-8984/19/50/506211)

J. Phys.: Condens. Matter **19** (2007) 506211 (15pp) doi:10.1088/0953-8984/19/50/506211

Chemical pressure and magnetic field effects in CePtGa

F C Ragel[1,2,3], P de V du Plessis[1,2] and A M Strydom[2]

[1] School of Physics, University of the Witwatersrand, Private Bag 3, PO WITS 2050, Johannesburg, South Africa
[2] Physics Department, University of Johannesburg, PO Box 524, Aucklandpark 2006, South Africa

E-mail: pdevduplessis@uj.ac.za

Received 9 July 2007, in final form 30 October 2007
Published 20 November 2007
Online at stacks.iop.org/JPhysCM/19/506211

Abstract

The antiferromagnetic Kondo compound CePtGa and the $Ce(Pt_{1-x}Ni_x)Ga$ and $CePt(Ga_{1-y}Al_y)$ alloy systems have been studied by resistivity $\rho(T)$, magnetoresistivity MR and susceptibility $\chi(T)$ measurements on polycrystalline samples to temperatures as low as 1.5 K and in magnetic fields up to 9 T. A Doniach diagram is presented of the volume dependences of the Néel temperature T_N and Kondo temperature T_K of these alloys and the possible existence of a quantum critical point near $x = 0.38$ is indicated. $\chi(T)$ measurements in different applied fields indicate a marked decrease in T_N with field for the parent CePtGa compound and extrapolation of the results suggests that magnetic order should disappear in a field of 4.8 T. In contrast the Kondo energy scale, identified by a maximum in $\rho(T)$ at low temperatures, increases significantly with field.

(Some figures in this article are in colour only in the electronic version)

1. Introduction

There has been considerable interest during the last decade in studying the behaviour of the equiatomic ternary Kondo compounds because of their variety of interesting ground-state properties, such as an insulating Kondo lattice ground state (e.g. CeNiSn [1] and CeRhSb [2]), ferromagnetic (e.g. CePdSb [3] and YbNiSn [4]) and antiferromagnetic (e.g. CePdGa [5], YbPtGa [6] and CePtGa [7, 8]) Kondo lattice behaviour, and heavy fermion behaviour (e.g. YbPdSb [9] and YbPtBi [10]). The orthorhombic TiNiSi-type (space group *Pnma*) structural compounds such as CePtGa [7, 8], CePdGa [5] and YbPtGa [6] show marked crystal-field interactions associated with the Kondo effect. The crystal symmetry plays a central role in determining the Kondo properties through the effect of the crystalline electric field (CEF) acting on the 4f orbitals. In this paper, the competing interplay between Kondo and Ruderman–Kittel–Kasuya–Yosida (RKKY) interactions in the CEF ground state is investigated as a function

[3] On leave from: The South Eastern University of Sri Lanka, Oluvil, Sri Lanka.

of chemical pressure and applied magnetic field in $Ce(Pt_{1-x}Ni_x)Ga$ ($0 \leqslant x \leqslant 0.5$) and $CePt(Ga_{1-y}Al_y)$ ($0 \leqslant y \leqslant 0.3$) alloys by electrical resistivity, magnetoresistance and magnetic susceptibility measurements.

The Néel temperature of the antiferromagnetic CePtGa compound has been observed as being in the range $T_N \approx 2.9$–3.5 K [7, 8, 11–13]. Electrical resistivity measurements $\rho(T)$ on polycrystalline [11] and single crystal [12] samples show a sharp drop below the Néel temperature. The $\rho(T)$ curves along the three principal axes of a single crystal sample show similar behaviour. Upon cooling from room temperature, $\rho(T)$ decreases linearly with a small gradient, and then shows a relatively sharp drop below 75 K and goes through a minimum at 23 K. Further cooling leads to a small increase in $\rho(T)$ before it goes through a maximum around 3.5 K and then drops suddenly below T_N [12]. The magnetic susceptibility $\chi(T)$ along the three principal axes also shows an anomaly at $T_N \approx 3.5$ K. $\chi(T)$ follows the Curie–Weiss law above 100 K, and the effective magnetic moments are reported to be 2.74, 2.89 and 2.70 μ_B/Ce ion for the *a*-, *b*- and *c*-axes [12]. An inelastic neutron scattering study shows two well-defined crystal field transitions around 209 and 413 K in the CePtGa compound [8]. These results show agreement with the estimate made by considering the effect of the crystal field on $\chi(T)$ of a single crystal [12]. Inelastic neutron scattering measurements and the results from magnetoresistance (MR) measurements suggest a Kondo temperature $T_K = 2.2$ K for the CePtGa compound [8].

$\rho(T)$ and MR measurements on the CePtGa compound have been reported under hydrostatic pressure [3, 11]. It is found through $\rho(T)$ measurements that T_N decreases with increasing pressure and disappears above 1 GPa. A maximum in the $\rho(T)$ curve is reported around 6 K at a pressure of 2 GPa, which suggests that a Kondo peak develops with increasing pressure. MR measurements at 4.2 K under various pressures suggest an incoherent Kondo state for lower pressures and then show a crossover at 3 GPa to the coherent state. Specific heat measurements on single crystal CePtGa show a λ-type anomaly at $T_N = 3.4$ K [13].

CePtAl, which has the same crystal structure as CePtGa, is reported to exhibit complex magnetic structures with magnetic phase transitions at $T_1 = 5.9$ K (second order), $T_2 = 4.3$ K (first order) and $T_3 = 2.2$ K (first order) [14]. A pronounced magnetic anisotropy is evident from susceptibility and magnetization measurements on CePtAl [15] and these results confirm the existence of a ferromagnetic component along the *a*-axis coexisting with incommensurate magnetic ordering in this compound [14]. An elaborate study of CeNiGa revealed intermediate valence behaviour for this compound which was changed upon hydrogenation of the material, giving a trivalent state for $CeNiGaH_{1.1}$ [16].

It is noted that our studies involve, for both alloy series, the substitution of elements belonging to the same column of the periodic table. Thus for $Ce(Pt_{1-x}Ni_x)Ga$ the d-electron count is invariant (Pt $5d^{10}$ replaced with Ni $3d^{10}$) and for $CePt(Ga_{1-y}Al_y)$ the p-electron count is invariant (Ga $4p^1$ replaced with Al $3p^1$). Consequently one may expect that volume changes induced by substitution, rather than electronic effects, will dominate the magnetic and Kondo behaviour of these alloys. A study of antiferromagnetic and Kondo behaviour in the related $Ce(Pt_{1-x}Pd_x)Ga$ system has recently been reported by Cho *et al* [17]. A preliminary report of our study of electrical properties of the $Ce(Pt_{1-x}Ni_x)Ga$ and $CePt(Ga_{1-y}Al_y)$ alloys has been recently published [18]. This work is extended in the present paper by magnetization and $\chi(T)$ studies, as well as a more detailed interpretation of the results.

2. Experimental details

Polycrystalline samples of $Ce(Pt_{1-x}Ni_x)Ga$ ($0 \leqslant x \leqslant 0.5$) and $CePt(Ga_{1-y}Al_y)$ ($0 \leqslant y \leqslant 0.5$) alloys were prepared using elements of the following purity in wt%: Ce, 99.98; Pt, 99.97; Ni,

99.99; Al, 99.999; Ga, 99.9999. Stoichiometric quantities of the constituent elements, but augmented by the addition of 2% of Ga to compensate for the possible loss of this low-melting temperature element, were arc-melted on a water-cooled copper hearth in a titanium-gettered ultra-pure argon atmosphere. The pieces of Ga were packed in the bottom and centre of the starting elements in the furnace and surrounded by the higher-melting-temperature elements, and arc-melting of the latter was initiated at low arc energies to allow for a slow reaction with the Ga. Melting three times with intermittent overturning of the ingot gave successful synthesis of alloy samples of typical mass 3 g. Weight loss ranged from 0.2–0.5 wt% of the total sample mass. Deviation from the stoichiometry of Ga content is estimated as within $\pm 1.5\%$, assuming that all of the weight loss is due to Ga evaporation. We did not anneal our samples in view of facilitating comparison between our results and those reported in the literature on an unannealed arc-melted CePtGa sample [11] and on unannealed single crystals of CePtGa grown by the Czochralski method in a tetra-arc furnace [12, 13].

Room-temperature x-ray powder diffraction measurements on the as-cast polycrystalline samples of the $Ce(Pt_{1-x}Ni_x)Ga$ and $CePt(Ga_{1-y}Al_y)$ alloys ascertained the phase purity of the samples and the absence of unreacted elements. The lattice parameters of the orthorhombic TiNiSi-type (space group *Pnma*) compounds were calculated using standard regression analysis of well-resolved peaks of the powder diffraction spectrum of each alloy.

$\rho(T)$ measurements were performed down to 1.5 K and isothermal MR measurements were performed up to 8 T. These transport measurements were done using a standard four-probe dc technique on bar-shaped samples (typical dimensions $6 \times 1 \times 1$ mm^3) cut by spark-erosion. The sample temperatures were varied and controlled between 1.5 K and room temperature using a variable-temperature insert and a temperature controller manufactured by Oxford Instruments.

Magnetization and susceptibility measurements were effected using the vibrating sample magnetometer option of the 9 T physical properties measurement system (PPMS) supplied by Quantum Design. Sample temperatures were varied and controlled in the range 1.9–400 K. Dimensions of typical samples used in these studies were $4 \times 1 \times 1$ mm^3. The magnetic field was applied along the long axis of a bar. For a selected number of samples isofield $\rho(T)$ measurements were performed down to 1.9 K for a number of fields up to 9 T using the PPMS.

3. Results and discussion

3.1. X-ray diffraction analysis

The variation of the room-temperature orthorhombic lattice parameters a, b and c and unit-cell volume V of as-cast samples of the alloy series $Ce(Pt_{1-x}Ni_x)Ga$, $(0 \leqslant x \leqslant 0.5)$ and $CePt(Ga_{1-y}Al_y)$ $(0 \leqslant y \leqslant 0.5)$ are shown in figure 1. The solid and dashed lines represent iterated least-squares fits to the data and illustrate that Vegard's rule is followed for these alloy systems in the investigated concentration ranges. The determined room-temperature orthorhombic lattice parameters of CePtGa, namely $a = 7.159(2) \times 10^{-1}$ nm, $b = 4.491(2) \times 10^{-1}$ nm and $c = 7.759(3) \times 10^{-1}$ nm, and the crystallographic unit-cell volume $V = 249.4(1) \times 10^{-3}$ nm are in agreement with the literature values of $a = 7.169 \times 10^{-1}$ nm, $b = 4.495 \times 10^{-1}$ nm and $c = 7.771 \times 10^{-1}$ nm^{-3} [12, 19]. The change in lattice parameters with y over the range $0 \leqslant y \leqslant 0.5$ extrapolates to lattice parameter values that are in agreement with previously reported values $a = 7.1980(4) \times 10^{-1}$ nm, $b = 4.4810(3) \times 10^{-1}$ nm and $c = 7.7956(4) \times 10^{-1}$ nm of a polycrystalline CePtAl sample [15]. Although an increase in the parameter a with x is observed in the $Ce(Pt_{1-x}Ni_x)Ga$ system, the other parameters b, c and V decrease as expected from the increasing Ni concentration x.

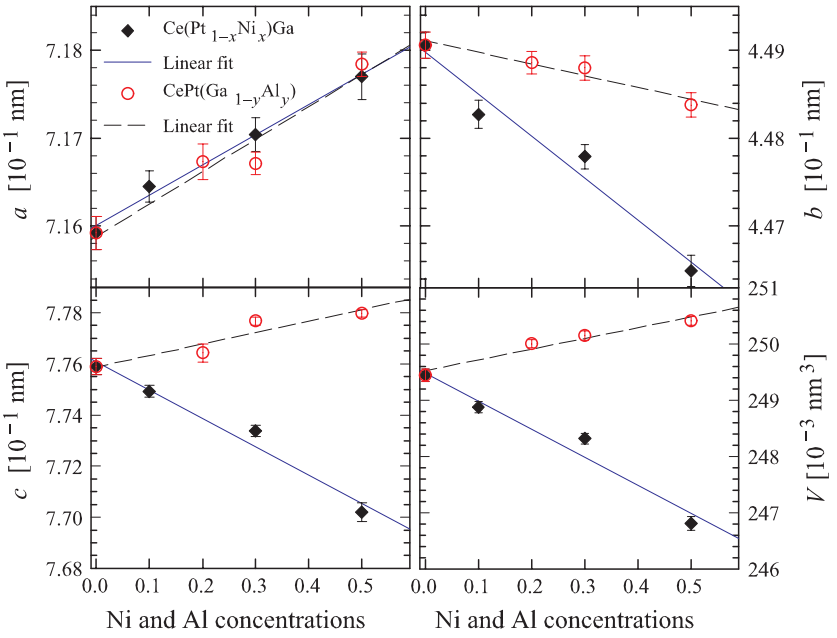

Figure 1. The orthorhombic lattice parameters a, b and c and unit-cell volume V of alloy compositions $0 \leqslant x \leqslant 0.5$ of the $Ce(Pt_{1-x}Ni_x)Ga$ system and $0 \leqslant y \leqslant 0.5$ of the $CePt(Ga_{1-y}Al_y)$ system.

3.2. Zero-field resistivity measurements

Normalized resistivity data $\rho(T)/\rho(280\ \mathrm{K})$ for the $Ce(Pt_{1-x}Ni_x)Ga$ and $CePt(Ga_{1-y}Al_y)$ alloys are depicted in figure 2. The inset shows the Kondo resistivity of the parent compound $\rho_{\mathrm{mag}}(T) = \rho_{\mathrm{CePtGa}}(T) - [\rho_{\mathrm{LaPtGa}}(T) - \rho_{\mathrm{LaPtGa}}(0)]$ plotted on a logarithmic temperature scale and of our LaPtGa sample plotted on a linear temperature scale. The observed $-\ln T$ dependence of $\rho_{\mathrm{mag}}(T)$ in two different temperature regimes is reminiscent of the behaviour of this quantity for several Ce systems, e.g. Ce_2Cu_2In, Ce_2Au_2In and Ce_2Pd_2In [20], $Ce_2Rh_3Ge_5$, $Ce_2Ir_3Ge_5$ [21] and $Ce_2Ni_3Ge_5$ [22]. Such temperature dependence originates due to the combined effect of Kondo and CEF interactions as treated by Cornut and Coqblin [23]. It is noted that the quantity $[\rho_{\mathrm{LaPtGa}}(T) - \rho_{\mathrm{LaPtGa}}(0)]$ reported by the authors of [12] for their polycrystalline sample is almost a factor of two larger than that observed in our studies. Using their results for LaPtGa either in conjunction with our polycrystalline CePtGa data or with their single-crystal data for CePtGa suitably averaged to simulate $\rho(T)$ for a polycrystalline sample, results in negative values of ρ_{mag} at 300 K, which seems to indicate that the results for $\rho(T)$ in [12] for LaPtGa are an over-estimate of the electron–phonon scattering contribution.

The maxima in the $\rho(T)$ data occurring at low temperatures are shown in more detail in figure 3. For CePtGa and for the $x = 0.2$, 0.3 and $y = 0.1$, 0.2 alloys these are associated with antiferromagnetic ordering. The Néel temperatures T_{N} are obtained through the line constructions as indicated in figure 3. For both the $Ce(Pt_{1-x}Ni_x)Ga$ and $CePt(Ga_{1-y}Al_y)$ alloy systems, a decrease in T_{N} is observed with increase in x or y. For higher Al concentrations the magnetic behaviour is more complex, as is evident from the occurrence of anomalies at two different temperatures in the $y = 0.3$ alloy, which may presumably be related to the complex magnetic behaviour reported for CePtAl [14, 15]. The maximum at T^{ρ}_{max} that appears in $\rho(T)$ for the $x = 0.5$ alloy is associated with its Kondo behaviour, since as will be evident from

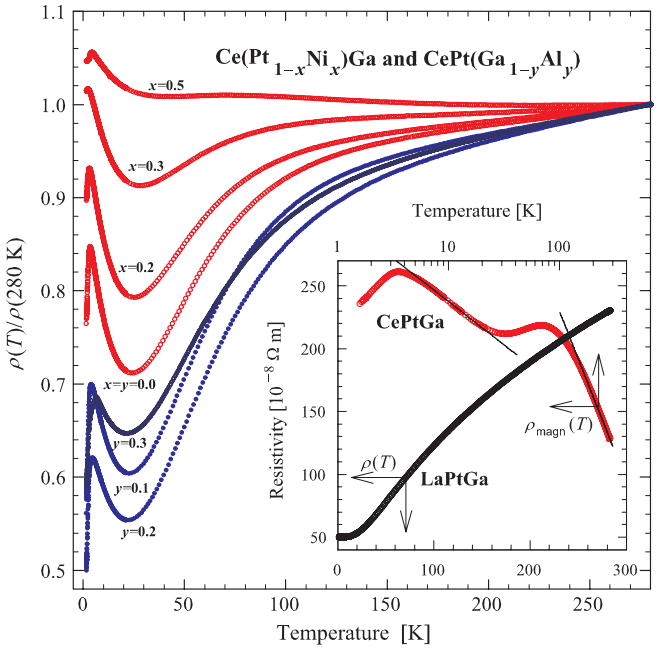

Figure 2. $\rho(T)/\rho(280\ \mathrm{K})$ of the systems $Ce(Pt_{1-x}Ni_x)Ga$ ($0 \leqslant x \leqslant 0.5$) and $CePt(Ga_{1-y}Al_y)$ ($0 \leqslant y \leqslant 0.3$). The inset shows the Kondo resistivity $\rho_{\mathrm{mag}}(T)$ of CePtGa and $\rho(T)$ of LaPtGa. The lines indicate the $\rho_{\mathrm{mag}}(T) \sim -\ln T$ behaviour in two temperature regimes.

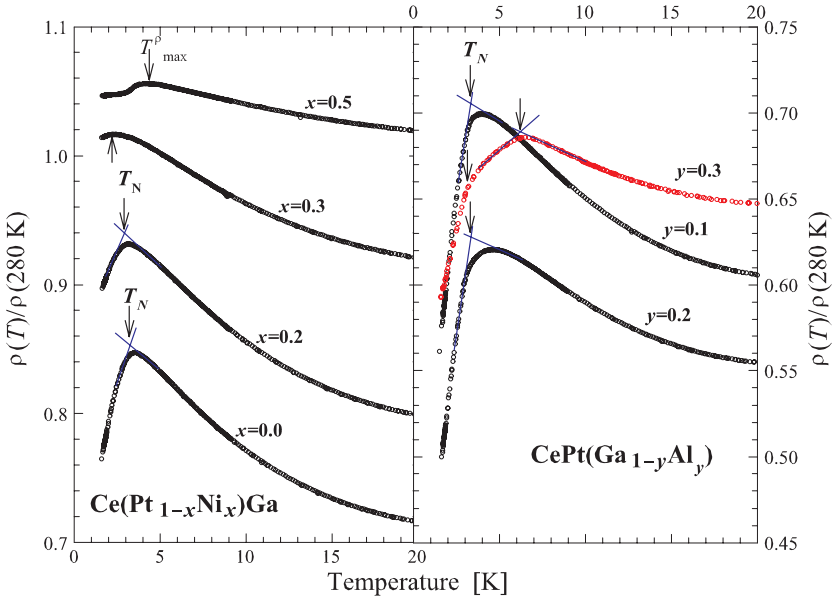

Figure 3. Temperature dependent normalized resistivities for the alloy compositions $0 \leqslant x \leqslant 0.5$ of the $Ce(Pt_{1-x}Ni_x)Ga$ system and $0 \leqslant y \leqslant 0.3$ of $CePt(Ga_{1-y}Al_y)$ shown in the temperature region $1.5\ \mathrm{K} \leqslant T \leqslant 20\ \mathrm{K}$.

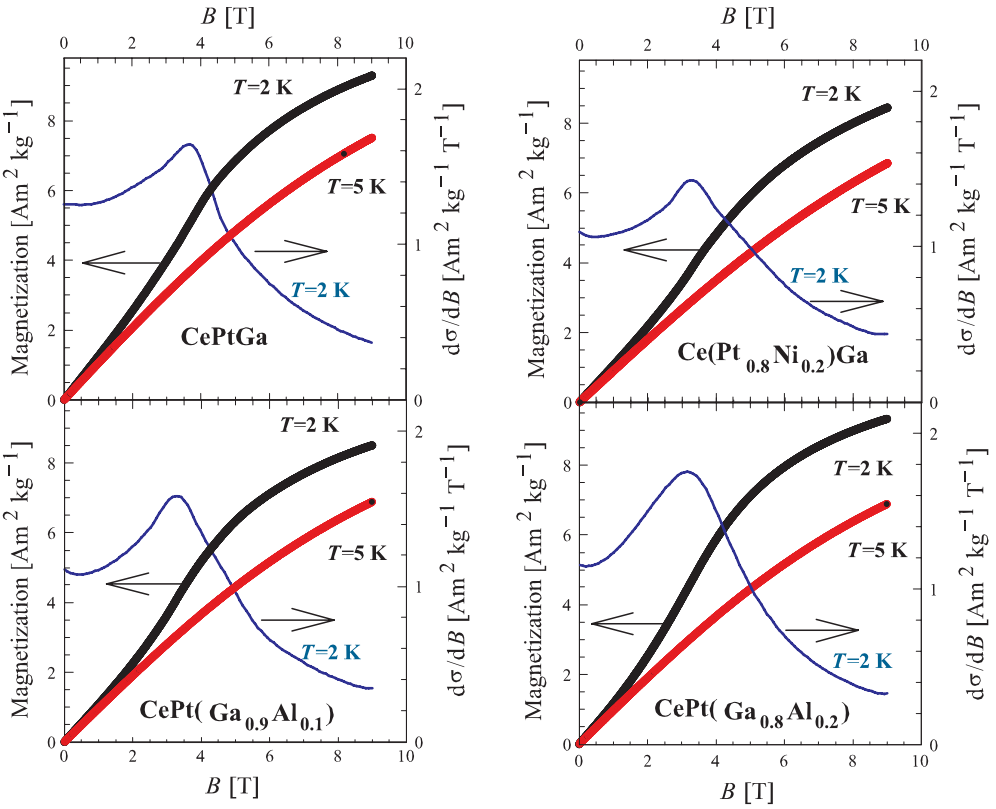

Figure 4. Magnetization measurements of CePtGa and of the $x = 0.2$, $y = 0.1$, 0.2 alloys at temperatures 2 and 5 K (left-hand scale). The right-hand scale shows the plot of $\mathrm{d}\sigma/\mathrm{d}B$ against the applied field $B = \mu_0 H$ (see text). The maximum of this plot indicates the field where a metamagnetic transition occurs.

section 3.5 the antiferromagnetic order disappears near $x = 0.38$. The magnetic phase diagram for the alloy systems is further investigated in the following sections through $\chi(T)$ and MR measurements.

3.3. Magnetization and susceptibility

Magnetization σ versus B isotherms measured at 2 K (i.e. below T_N) and at 5 K (i.e. above T_N) are shown in figure 4 for CePtGa and a representative selection of alloy samples (we assume $B = \mu_0 H$ throughout this paper for the sake of simplicity). Evidence of metamagnetic behaviour is seen for our polycrystalline CePtGa sample in confirmation of the metamagnetic behaviour of the c-axis magnetization observed in single crystal CePtGa [12]. A maximum in $\mathrm{d}\sigma/\mathrm{d}B$ indicative of the metamagnetic transition occurs for our 2 K isotherm at 3.6 T, which is in good agreement with a metamagnetic transition which occurs at 3.5 T along the c-axis of the CePtGa single crystal at 2 K [12]. Metamagnetic behaviour is also evident for the 2 K magnetization isotherms for the other alloy samples in figure 4.

Susceptibility $\chi(T)$ measurements performed in a field of 0.1 T are presented in figure 5. The curves for CePtGa and for the alloys with $x = 0.2$, 0.3 and $y = 0.1$, 0.2 confirm the antiferromagnetic order observed in $\rho(T)$ measurements. For the $y = 0.3$ alloy the $\chi(T)$ curve

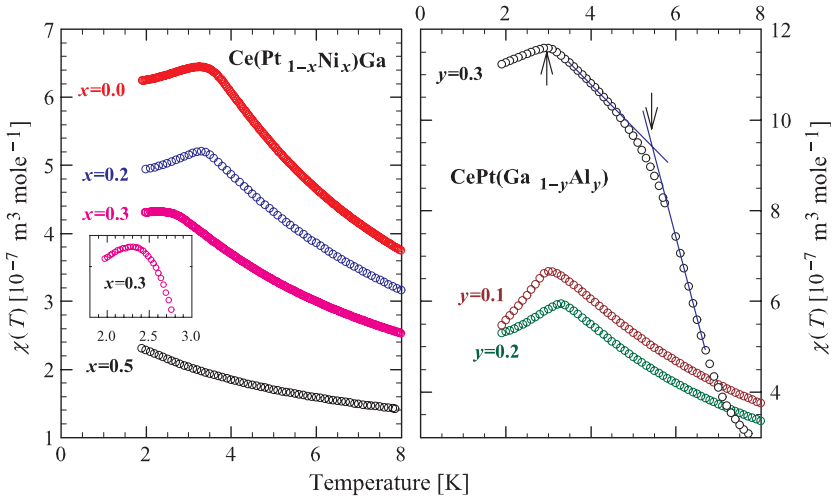

Figure 5. Susceptibility $\chi(T)$ measurements between 8 and 1.9 K in an applied field of 0.1 T. The Néel temperature is taken at the peak in $\chi(T)$. For $y = 0.3$ two anomalies are evident around 3 and 6 K as also observed in $\rho(T)$ in figure 3, presumably associated with the complex behaviour of CePtAl (see text).

shows an indication of two transitions at temperatures similar to the anomalies indicated in the $\rho(T)$ data for this sample. Because of this more complex behaviour observed for the $y = 0.3$ alloy, which may be related to the intricate properties of CePtAl [14], our further investigation and interpretations are confined to the CePtGa compound and the alloys $0.1 \leqslant x \leqslant 0.5$ and $y = 0.1, 0.2$. For these alloys it is seen that substitution of Ni for Pt, as well as Al for Ga, decreases T_N from the value $T_N = 3.25$ K observed for the parent CePtGa compound. The variation of T_N for these alloys as observed from $\chi(T)$ and from $\rho(T)$ data is depicted in figure 9 in section 3.5 as a function of unit-cell volume, and this dependence is discussed in that section.

Results of $\chi^{-1}(T)$ for the two alloy systems are plotted in figure 6. The plot conforms well with the expected Curie–Weiss behaviour $\chi^{-1}(T) = 3k_B(T - \theta_P)/N_A\mu_{eff}$ over most of the temperature range, but deviations from linearity are evident at lower temperatures. Linear least-squares (LSQ) fits for the data of figure 6 in the temperature region 150–400 K yield values of θ_P and μ_{eff} as given in table 1. The effective moment value for CePtGa is slightly higher than the free Ce^{3+} ion value of 2.54 μ_B, but is in agreement with μ_{eff} values observed for a single crystal of CePtGa [12].

3.4. Magnetoresistance

Magnetoresistance (MR) isotherms were measured in transverse fields up to 8 T for a number of alloys. A typical example of the results is shown in figure 7 for the $Ce(Pt_{0.8}Ni_{0.2})Ga$ sample. Results taken during increasing fields always fall on the same curve as data taken during decreasing fields. The behaviour in figure 7 is typical of the suppression of incoherent Kondo scattering in a magnetic field. The data, except for isotherms near T_N, can be fitted to the results of the Bethe ansatz calculations of the Coqblin–Schrieffer model as predicted by Andrei [24] and Schlottmann [25]

$$\frac{\rho(B)}{\rho(0)} = \left[\frac{1}{2j+1}\sin^2\left(\frac{\pi n_f}{2j+1}\right)\sum_{\ell=0}^{2j}\sin^{-2}(\pi n_\ell)\right]^{-1}. \quad (1)$$

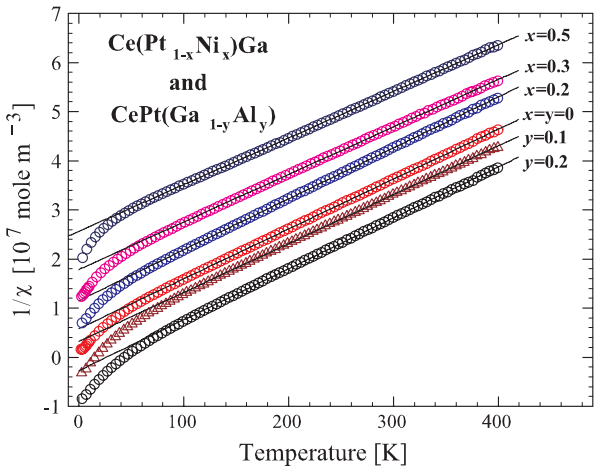

Figure 6. Plot of $\chi^{-1}(T)$ of CePtGa and the alloy compositions $x = 0.2, 0.3, 0.5$ and $y = 0.1, 0.2$ in the temperature range 400–1.9 K. The solid line LSQ fits are for data in the temperature region 150–400 K. Note the offset in $1/\chi$ values amounting to 0.5, 1.0 and 1.5×10^7 mol m^{-3} for $x = 0.2$, 0.3 and 0.5, respectively, and -0.5 and -1.0×10^7 mol m^{-3} for $y = 0.1$ and 0.2, respectively.

Table 1. The paramagnetic Curie temperature θ_P and effective magnetic moment μ_{eff} were obtained by LSQ fits of the Curie–Weiss relation to the $\chi^{-1}(T)$ data in figure 6. The fits are shown by solid lines (see text).

$Ce(Pt_{1-x}Ni_x)Ga$ and $CePt(Ga_{1-y}Al_y)$	$-\theta_P$ (K)	μ_{eff} (μ_B/Ce)
$x = y = 0$	57.3	2.76(2)
$x = 0.2$	62.9	2.75(2)
$x = 0.3$	81.4	2.79(3)
$x = 0.5$	112.3	2.81(2)
$y = 0.1$	82.9	2.77(3)
$y = 0.2$	70.4	2.75(3)

Since inelastic neutron scattering data on CePtGa display two well-defined crystal-field levels at 209 and 413 K which are well separated from the ground-state doublet, our system may be treated at low temperatures as a $j = \frac{1}{2}$ Ce impurity system [8]. The solid lines in figure 7 are LSQ fits for the $j = \frac{1}{2}$ case of (1) to the experimental data. It is noted that the isotherms at 1.5 and 3 K which are near T_N deviate from equation (1) as indicated by dotted curves in figure 7. The exact solutions for $j = \frac{1}{2}$ in the above model indicate that the MR is completely determined by a single parameter, the characteristic field B^* [25], which is expected to have the following temperature dependence [26]

$$B^*(T) = B^*(0) + \frac{k_B T}{g\mu_K} = \frac{k_B(T_K + T)}{g\mu_K}. \tag{2}$$

Values of $B^*(T)$ obtained from the LSQ fits of (1) to the data in the main figure, are plotted in the inset in figure 7. The linear relation predicted by (2) is borne out at low temperature, but there is some deviation from linearity from the B^* values of the 23 and 30 K isotherms which may be associated with an increased population of the first excited crystal-field level with increasing temperature. A LSQ fit of (2) to the $B^*(T)$ points yields $B^*(0)$, hence T_K, and also the corresponding magnetic moment μ_K of the Kondo ion. Values of T_K and μ_K thus

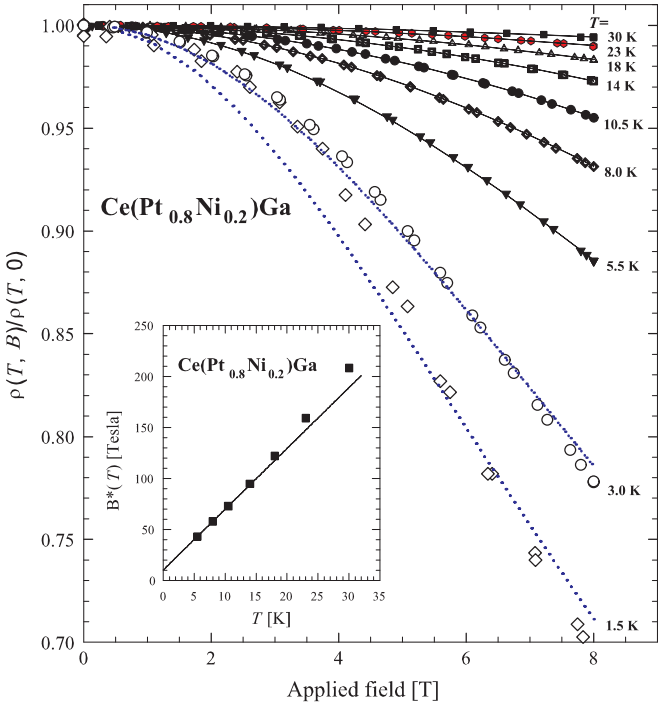

Figure 7. The magnetic field dependence of electrical resistivity at a number of sample temperatures for the alloy $Ce(Pt_{0.8}Ni_{0.2})Ga$. The data were measured in increasing and decreasing fields without evidence of hysteresis. The solid curves in the main figure are LSQ fits of the Bethe ansatz theory of magnetoresistance (equation (1)) to the experimental data. The inset shows the temperature variation of the characteristic field $B^*(T)$, and the line is a LSQ fit of equation (2) to the B^* values.

Table 2. Values of Kondo temperature T_K and the magnetic moment of the Kondo ion μ_K as obtained from fits of equations (1) and (2) to the magnetoresistance data of several $Ce(Pt_{1-x}Ni_x)Ga$ and $CePt(Ga_{1-y}Al_y)$ alloys.

$Ce(Pt_{1-x}Ni_x)Ga$ and $CePt(Ga_{1-y}Al_y)$	T_K (K)	μ_K (μ_B/Ce)
$x = y = 0$	1.1(2)	0.128(3)
$x = 0.2$	1.74(7)	0.125(1)
$x = 0.3$	2.39(4)	0.0874(5)
$x = 0.5$	5.6(2)	0.070(1)
$y = 0.1$	1.0(2)	0.133(3)
$y = 0.2$	0.8(3)	0.144(5)

obtained for the investigated alloys are given in table 2. The evolution of T_K through the alloy systems is discussed in section 3.5. The observed values of μ_K are appreciably reduced from the paramagnetic μ_{eff} values given in table 1.

Finally, it is shown in figure 8 that the combined data for the $Ce(Pt_{1-x}Ni_x)Ga$ and the $CePt(Ga_{1-y}Al_y)$ systems conform to the universal scaling of $B^*(T)$. Data for isotherms between 5.5 and 10.5 K for the concentrations $x = 0$, 0.2, 0.3 and 0.5 as well as for $y = 0.1$ and 0.2 all fall on one curve. A related scaling behaviour encompassing both the $x = 0$ and $x = 0.5$ members of the $Ce(Pt_{1-x}Ni_x)Sn$ alloy system has been previously reported [27].

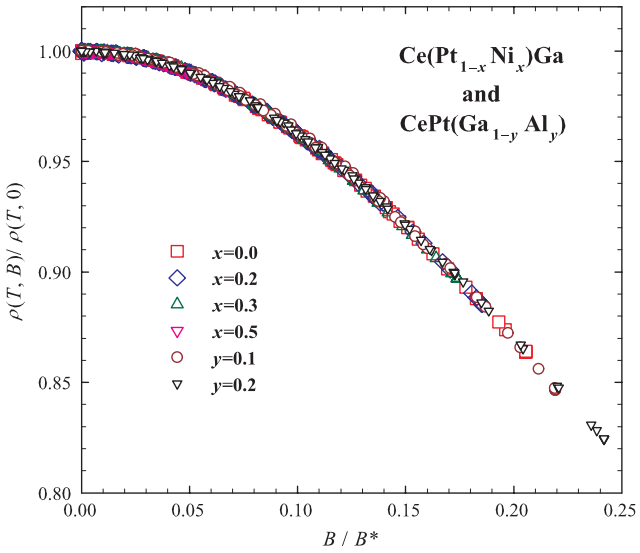

Figure 8. The universal scaling of $B^*(T)$ observed for both the $Ce(Pt_{1-x}Ni_x)Ga$ and $CePt(Ga_{1-y}Al_y)$. Data for isotherms between 5.5 and 10.5 K for the concentrations $x = 0, 0.2, 0.3$ and 0.5 as well as for $y = 0.1$ and 0.2 all fall on one curve.

3.5. Volume dependence of T_N and T_K

Values of T_N for the alloy systems as deduced from $\rho(T)$ measurements (figure 3) and $\chi(T)$ measurements (figure 5) are shown in figure 9(a) as a function of hydrostatic pressure and change in unit-cell volume. It is also noted that measurements performed by us of the specific heat C_P at low temperatures on the parent CePtGa compound indicate a peak in C_P at 3.1 K which confirms the antiferromagnetic ordering of the compound and is in satisfactory agreement with $T_N = 3.25$ K observed from $\chi(T)$ measurements. The linear Vegard rule dependences of unit-cell volume V on x and y have been used to construct a unified scale of cell volume encompassing both alloy systems, which is plotted on the lower horizontal axis of figure 9(a). The variation of T_N with hydrostatic pressure has been reported by Uwatoko *et al* for CePtGa [13]. In figure 9(a) we scale the T_N data from our alloying experiments and the T_N data from the pressure studies so as to collapse the two sets of data on a single curve. The scaling implies a bulk modulus of 160 GPa for CePtGa, which is comparable with bulk modulus values observed in several Ce Kondo compounds [28]. Moreover, the horizontal axis scaling enables comparison with the conventional Doniach [29] and Brandt and Moschchalkov [30] diagrams in which $|JN(E_F)|$ increases along the horizontal axis. J is the Kondo coupling constant and $N(E_F)$ denotes the density of states at the Fermi level. By extrapolation, T_N is expected to vanish for a pressure of ≈1.2 GPa applied to CePtGa or at a unit-cell volume of $\approx 247.6 \times 10^{-3}$ nm^3 in the $Ce(Pt_{1-x}Ni_x)Ga$ system which corresponds to a value of $x \approx 0.38$. Quantum critical behaviour is expected for alloys near this concentration. A more detailed study of the phase diagram utilizing lower temperatures is called for in this region.

The scaling also facilitates the study of the variation of the Kondo energy scale $T_K(\propto T^{\rho}_{max})$ with regard to the compressible Kondo lattice (CKL) model [31, 32] in figure 9(b). The CKL model for Ce compounds gives the volume dependence of $|JN(E_F)|$ as $|JN(E_F)| = |JN(E_F)|_0 \exp[-q(V - V_0)/V_0]$, where $|JN(E_F)|_0$ indicates the value of the quantity at initial volume V_0, and q refers to the Grüneisen parameter of $|JN(E_F)|$

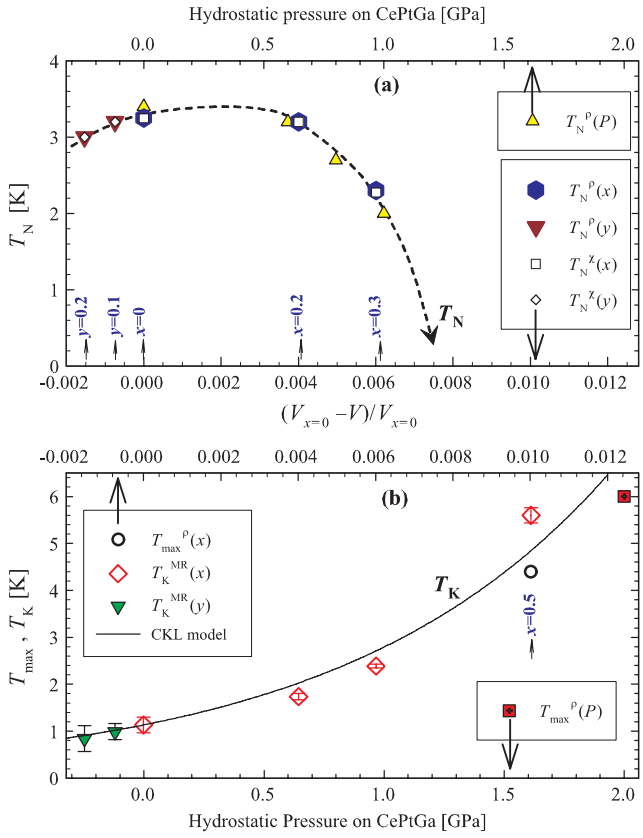

Figure 9. Néel temperatures T_N^{ρ} and T_N^{χ} obtained from $\rho(T)$ and $\chi(T)$ measurements, as well as the Kondo resistivity peak T_{max}^{ρ} from $\rho(T)$ measurements and the Kondo temperatures T_K from MR measurements plotted against hydrostatic pressure on the CePtGa compound (taken from [13]) and $(V_{x=0} - V)/V_{x=0}$ of the $Ce(Pt_{1-x}Ni_x)Ga$ ($0 \leqslant x \leqslant 0.5$) and $CePt(Ga_{1-y}Al_y)$ ($0 \leqslant y \leqslant 0.2$) systems. The solid curve in (b) is a LSQ fit of equation (3) to the data points. Superimposing (a) and (b) resembles a Doniach phase diagram.

(i.e. $q = -\partial \ln |JN(E_F)|/\partial \ln V$) [33] and is considered to vary between 6 and 8 [31, 34]. Since $T_K \propto \exp(-1/|JN(E_F)|)$ the volume dependence of T_K may be described by

$$T_K(V) = T_K(V_{x=0}) \exp\left[\frac{q(V_{x=0} - V)}{|JN(E_F)|_{x=0}\, V_{x=0}}\right] \tag{3}$$

as a function of the concentration dependent volume (see [33–35]). We apply (3) to the results of alloy compositions $0 \leqslant x \leqslant 0.5$ and $0.1 \leqslant y \leqslant 0.2$ of the $Ce(Pt_{1-x}Ni_x)Ga$ and $CePt(Ga_{1-y}Al_y)$ systems. The exponential solid line in figure 9(b) is a LSQ fit of (3) with $q = 6$ to the T_{max} and T_K values plotted in the figure. This gives $|JN(E_F)|_{x=0} = 0.041 \pm 0.001$ for the parent compound CePtGa. Such a value for the CePtGa compound which has a small $T_K = 1.1 \pm 0.2$ K value is in agreement with a comparison of previously reported $|JN(E_F)|$ values of several compounds when scaled according to the Doniach model (figure 10 in [36]). We have calculated the value of the electronic Grüneisen parameter $\Omega_e = -\partial(\ln T_K)/\partial(\ln V)$ [28] using the data given in figure 9(b) and obtained $\Omega_e = 146 \pm 8$. We note that large values of Ω_e are often associated with heavy-fermion compounds, e.g. $CeCu_6$ with a γ-coefficient of 1600 mJ mol^{-1} K^{-2} has $\Omega_e = 110$ [28]. In comparison the mixed-valent

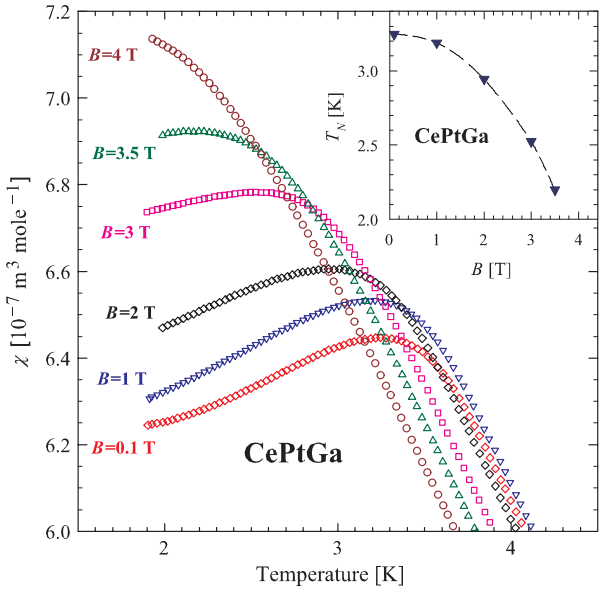

Figure 10. $\chi(T)$ of CePtGa measured for different applied fields. The maxima in $\chi(T)$ give values of $T_N(B)$ which are plotted in the inset to the figure.

compound $CeSn_3$ has $\gamma = 10$ mJ mol^{-1} K^{-2} and $\Omega_e = 11$ [28]. Antiferromagnetic ordering at $T_N \approx 3.4$ K complicates the determination of γ from low-temperature heat capacity data of CePtGa [13, 17]. From an analysis of paramagnetic heat capacity results ($T \geqslant 8$ K) a value of $\gamma = 58$ mJ mol^{-1} K^{-2} was deduced [17], whereas the authors of [13] suggested that the large value of $C/T \approx 400$ mJ mol^{-1} K^{-2} observed at 0.3 K, which is well below T_N, may indicate the heavy-fermion character of the compound. It should be noted that the association of a large Ω_e value with extreme values of γ is not always observed, e.g. $CeRu_2Si_2$ with a large $\Omega_e = 175$ is only a moderate heavy-fermion compound with $\gamma = 385$ mJ mol^{-1} K^{-2}. Theoretical studies by Burdin *et al* [37] indicate an enhanced T_K in the vicinity of a quantum critical point. Thus, the possible occurrence of quantum criticality as suggested from our results may concur with the large Ω_e value found for CePtGa.

3.6. Field dependence of T_N and T_{max}

Low temperature $\chi(T)$ measurements for the CePtGa compound are depicted in figure 10 for different values of applied field. The maximum in $\chi(T)$ which is taken as an indication of the Néel temperature T_N is observed to decrease markedly with application of the field as depicted in the inset in figure 10.

In figure 11 the normalized zero-field resistivities of the $Ce(Pt_{1-x}Ni_x)Ga$ alloys with $x = 0$, 0.3 and 0.5 are compared with normalized isofield resistivity data of these alloys. Isofield measurements were also taken for alloys with $y = 0.1$ and 0.2, but since the results are similar to those for the $x = 0$ and 0.3 alloys, the results for the former alloys are not presented here.

It is observed that the maximum in the zero-field $\rho(T)$ curve of CePtGa is progressively shifted to higher temperatures for larger fields. Values of $T_{max}(B)$ deduced from the data in figure 11 are depicted in figure 12(a). Also shown in this figure are values of $T_N(B)$ observed from the $\chi(T)$ measurements in figure 10. A tentative extrapolation of the decrease in $T_N(B)$

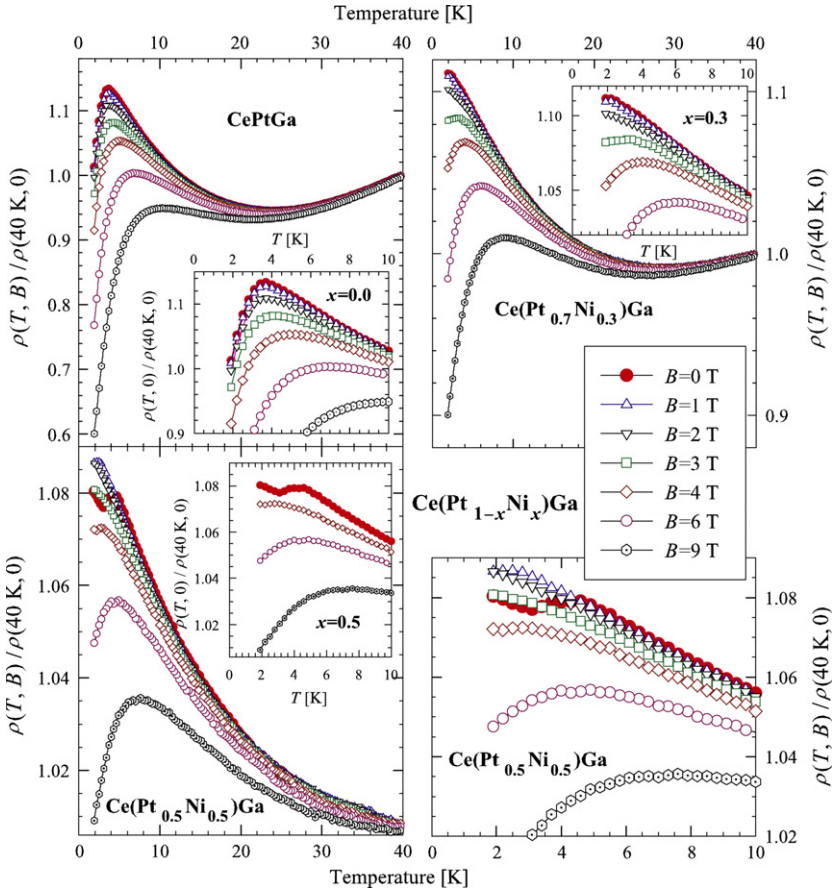

Figure 11. Normalized isofield resistivity curves for $Ce(Pt_{1-x}Ni_x)Ga$ alloys ($x = 0$, 0.3, 0.5). Maxima in the zero-field curves are in general displaced to higher temperatures with application of the field. For the $x = 0.5$ alloy the results at low fields and temperatures are more complicated.

predicts that the magnetic order should disappear in a field of about 4.8 T. It would be of interest to extend measurements to lower temperatures in order to establish whether a field-induced QCP exists in this material. It is seen from figure 9(a) that T_N values obtained from $\rho(T)$ through the construction in figure 3 and from the peaks in $\chi(T)$ data in $B = 0.1$ T are in agreement, and show a change in T_N with volume. When a field is applied, $\chi(T)$ through its peak values traces the decrease of $T_N(B)$ as seen in figure 10. However $\rho(T)$ of CePtGa behaves differently in that an increase in T_{max} is observed as indicated in figure 12(a). These observed T_{max} values should be regarded as indicative of the Kondo scale, $T_{max}(B) \propto T_K^B$. The value of T_K as calculated from the MR measurements in section 3.4 is regarded as representative of $B = 0$ for the system since the Schlottmann analysis yields values of $B^*(T)$ independent of the field range used (see the theoretical fits to the experimental data in figure 7). The value of T_K as measured by MR can be connected smoothly to T_{max} values ($3\ T \leqslant B \leqslant 9\ T$) as indicated by the dashed line in figure 12(a). It is surmised that the T_{max} values at lower fields deviate from the dashed line because magnetic ordering sets in at a higher temperature than T_K for this material, thus possibly distorting the Kondo peak. The interplay of T_N and the Kondo energy scale (T_{max}, T_K) in figure 12(a) has the characteristics of a Doniach diagram.

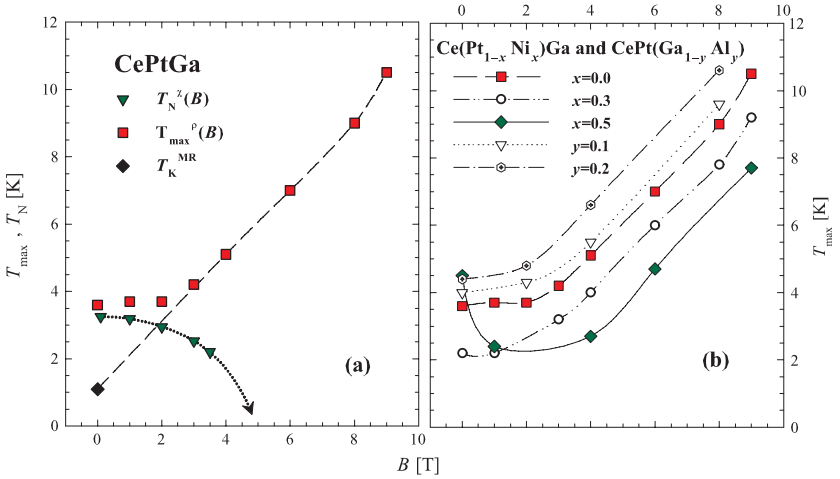

Figure 12. (a) The field dependence of $T_{max}(\propto T_K^B)$ and of T_N for CePtGa and (b) the field dependence of $T_{max}(\propto T_K^B)$ for the Ce($Pt_{1-x}Ni_x$)Ga and CePt($Ga_{1-y}Al_y$) systems.

It is shown in figure 12(b) that for the alloys $x = 0$ and 0.3 (for which the isofield resistivity curves are shown in figure 11) and $y = 0.1$ and 0.2 (for which our isofield data are not shown) the resistivity maxima show a monotonic increase with field. An exception to this is the results for the $x = 0.5$ alloy where an initial decrease in T_{max} with increase in field is observed. This originates from the behaviour of the zero- and low-field curves for this alloy at low temperatures as indicated in figure 11 and for which we do not have an explanation at present. An increase of T_{max} is observed in isofield resistivity studies of several Kondo systems [38] and is also in accord with theoretical considerations [39].

4. Conclusion

Our experimental study clearly illustrates the competing interplay between Kondo and magnetic interactions in CePtGa and in the Ce($Pt_{1-x}Ni_x$)Ga and CePt($Ga_{1-y}Al_y$) alloy systems. From the parameters $T_K(\propto T_{max})$ and T_N observed in our experiments a Doniach diagram for the alloy system suggests the possible existence of a QCP near $x = 0.38$. When Pd is substituted for Pt in the CePtGa compound [17] it is found that antiferromagnetic ordering is observed over the complete substitution range between CePtGa ($T_N = 3.4$ K) and CePdGa ($T_N = 1.3$ K). Therefore substitution of Pt with the smaller Ni atoms is a requisite to drive the system to a possible QCP. For the parent compound it is shown that application of a field markedly decreases T_N and extrapolation indicates it to disappear at 0 K in a field of about 4.8 T. Detailed measurements at lower temperatures would be of considerable interest for investigating the possible existence and characteristics of a QCP in the alloy system at $x \approx 0.38$ and the possible existence of a field-induced QCP for CePtGa near 4.8 T.

Acknowledgments

Support by the South African National Research Foundation (NRF) through grants GUN 2053778 and GUN 2072956 and the universities of the Witwatersrand and of Johannesburg are acknowledged. Dr M B Tchoula Tchokonté is thanked for assisting with the x-ray diffraction measurements. F C Ragel wishes to thank the NRF and Wits University for granting bursaries

for the study, and the University of Johannesburg for funding a recent visit to its physics department. He also extends his appreciation to the South Eastern University of Sri Lanka for granting leave to pursue his research in South Africa.

References

[1] Takabatake T, Teshima F, Fujii H, Nishigori S, Suzuki T, Fujita T, Yamaguchi Y, Sakurai J and Jaccard D 1990 *Phys. Rev.* B **41** 9607
[2] Malik S K and Adroja D T 1991 *Phys. Rev.* B **43** 6277
[3] Malik S K and Adroja D T 1991 *Phys. Rev.* B **43** 6295
[4] Bonville P, Bellot P, Hodges J A, Imbert P, Jéhanno G, Le Bras G, Hammann J and Leylekian L 1992 *Physica* B **182** 105
[5] Adroja D T, Rainford B D and Malik S K 1994 *Physica* B **194–196** 169
[6] Adroja D T, Rainford B D, Malik S K, Gailloux M and Gschneidner K A Jr 1994 *Phys. Rev.* B **50** 248
[7] Fujita T, Suzuki T, Nishigori S, Takabatake T, Fujii H and Sakurai J 1992 *J. Magn. Magn. Mater.* **108** 35
[8] Adroja D T, Rainford B D and Neville A J 1996 *Physica* B **223/224** 279
[9] Dhar S K, Nambudripad N and Vijayaraghavan R 1988 *J. Phys. F: Met. Phys.* **18** L41
[10] Fisk Z, Canfield P C, Beyermann W P, Thompson J D, Hundley M F, Ott H R, Felder E, Maple M B, Lopez de la Torre M A, Visani P and Seaman C L 1991 *Phys. Rev. Lett.* **67** 3310
[11] Uwatoko Y, Ishii T, Oomi G and Malik S K 1995 *Physica* B **206/207** 199
[12] Shirakawa M, Kasaya M, Uwatoko Y, Oomi G and Môri N 2000 *Physica* B **281/282** 94
[13] Uwatoko Y, Kosaka M, Shirakawa M, Oomi G, Môri N, Kobayashi T, Tatewaki H, Shimizu K and Amaya K 2000 *Physica* B **284&288** 1321
[14] Dönni A, Kitazawa H, Fischer P, Tang J, Kohgi M, Endoh Y and Morii Y 1995 *J. Phys.: Condens. Matter* **7** 1663
[15] Kitazawa H, Nimori S, Tang J, Iga F, Dōnni A, Matsumoto T and Kido G 1997 *Physica* B **237/238** 212
[16] Chevalier B, Bobet J-L, Gaudin E, Pasturel M and Etourneau J 2002 *J. Solid State Chem.* **168** 28
[17] Cho H H, Lee W H and Chen Y Y 2004 *Solid State Commun.* **130** 821
[18] Ragel F C, Du Plessis P de V and Strydom A M 2007 *J. Magn. Magn. Mater.* **310** 365
[19] Hovestreydt E, Engel N, Klepp K, Chabot B and Parthé E 1982 *J. Less-Common Met.* **85** 247
[20] Kaczorowski D, Rogl P and Hiebl K 1996 *Phys. Rev.* B **54** 9891
[21] Hossain Z, Ohmoto H, Umeo K, Iga F, Suzuki T, Takabatake T, Takamoto N and Kindo K 1999 *Phys. Rev.* B **60** 10383
[22] Hossain Z, Hamashima S, Umeo K, Takabatake T, Geibel C and Steglich F 2000 *Phys. Rev.* B **62** 8950
[23] Cornut B and Coqblin B 1972 *Phys. Rev.* B **5** 4541
[24] Andrei N 1982 *Phys. Lett.* A **87** 299
[25] Schlottmann P 1983 *Z. Phys. B: Condens. Matter* **51** 223
[26] Batlogg B, Bishop D J, Bucher E, Golding B Jr, Ramirez A P, Fisk Z, Smith J L and Ott H R 1987 *J. Magn. Magn. Mater.* **63/64** 441
[27] Adroja D T, Rainford B D, Neville A J and Jansen A G M 1996 *Physica* B **223/224** 275
[28] Thompson J D and Lawrence J M 1994 *Handbook on the Physics and Chemistry of Rare Earths* vol 19, ed K A Gschneidner Jr, E LeRoy, G H Lander and G R Choppin (Amsterdam: Elsevier) p 383
[29] Doniach S 1977 *Physica* B **91** 231
[30] Brandt N B and Moshchalkov V V 1984 *Adv. Phys.* **33** 373
[31] Lavagna M, Lacroix C and Cyrot M 1982 *Phys. Lett.* A **90** 210
[32] Lavagna M, Lacroix C and Cyrot M 1983 *J. Phys. F: Met. Phys.* **13** 1007
[33] Bauer E, Hauser R, Gratz E, Payer K, Oomi G and Kagayama T 1993 *Phys. Rev.* B **48** 15873
[34] Kagayama T, Oomi G, Takahashi H, Mōri N, Ōnuki Y and Komatsubara T 1991 *Phys. Rev.* B **44** 7690
[35] Umeo K, Kadomatsu H and Takabatake T 1996 *Phys. Rev.* B **54** 1194
[36] Ragel F C and Du Plessis P de V 2004 *J. Phys.: Condens. Matter* **16** 2647
[37] Burdin S, Grempel D R and Georges A 2002 *Phys. Rev.* B **66** 045111
[38] Felsch W and Winzer K 1973 *Solid State Commun.* **13** 569
Remenyi G, Jaccard D, Flouquet J, Briggs A, Fisk Z, Smith J L and Ott H R 1986 *J. Physique* **47** 367
Thompson J D, Mc Elfresh M W, Willis J O, Fisk Z, Smith J L and Maple M B 1987 *Phys. Rev.* B **35** 48
[39] Bloomfield P E, Hecht R and Sievert P R 1970 *Phys. Rev.* B **2** 3714
Ruvalds J and Sheng Q G 1988 *Phys. Rev.* B **37** 1959
Tian D P and Keiter H 1973 *Solid State Commun.* **13** 569
Rozhavsky A S, Zagoskin A M, Naidyuk Y G and Tuluzov I G 1992 *Phys. Rev.* B **46** 14903